

1 **Development of Equine Polyclonal Antibodies as a Broad-Spectrum Therapy Against**
2 **SARS-CoV-2 Variants**

3

4 Shumin Liao^{1,2,3*}, Yunjiao He^{1*}, Jing Qu^{4*}, Yue Shi¹, Yingzi Liu^{5,1}, Keli Zhao⁵, Junhui Chen⁵,
5 Yue Jing^{6,7,8}, Clifton Kwang-Fu Shen^{6,7,8,9}, Chong Ji^{6,7,8}, Guxun Luo^{6,7,8}, Xusheng Zhao^{6,7,8},
6 Shuo Li^{10,11}, Yunping Fan³, Ziquan Lv⁴, Shisong Fang⁴, Yaqing He⁴, Chunli Wu⁴, Renli Zhang⁴,
7 Xuan Zou^{4#}, Peng Wang^{1#}, Liang Li^{1,12#}

- 8 1. School of Medicine, Southern University of Science and Technology, Shenzhen, China
9 2. Department of Thoracic Surgery, The Seventh Affiliated Hospital of Sun Yat-sen
10 University, Shenzhen, China
11 3. Department of Otolaryngology, The Seventh Affiliated Hospital of Sun Yat-sen University,
12 Shenzhen, China
13 4. Shenzhen Center for Disease Control and Prevention, No. 8, Longyuan Road, Nanshan
14 District, Shenzhen, Guangdong Province, China
15 5. Peking University Shenzhen Hospital, No. 1120, Lianhua Road, Futian District, Shenzhen,
16 China
17 6. Jiangxi Institute of Biological Products Co. Ltd., Jiangxi, China
18 7. Jiangxi Institute of Biological Products Shenzhen R&D Center Co. Ltd., Shenzhen, China
19 8. Hainan Institute of Pharmaceutical Research Co. Ltd., Hainan, China
20 9. SUSTech Academy for Advanced Interdisciplinary Studies, Southern University of
21 Science and Technology, Shenzhen, China
22 10. Huazhong University of Science and Technology Union Shenzhen Hospital, Shenzhen,
23 China
24 11. The Sixth Affiliated Hospital of Shenzhen University Health Science Center, Shenzhen,
25 China
26 12. Institute of Biomedicine and Biotechnology, Shenzhen Institute of Advanced Technology,
27 Chinese Academy of Sciences, Nanshan, Shenzhen, China

28

29 *Equal contribution

30 # Corresponding authors:

31 Liang Li (lil@sustech.edu.cn), Peng Wang (wangp6@sustech.edu.cn), and Xuan Zou
32 (1229346705@qq.com)

33

34 **Abstract**

35 The Coronavirus disease 19 (COVID-19) pandemic has accumulated over 550 million
36 confirmed cases and more than 6.34 million deaths worldwide. Although vaccinations has
37 largely protected the population through the last two years, the effect of vaccination has been
38 increasingly challenged by the emerging SARS-CoV-2 variants. Although several therapeutics
39 including both monoclonal antibodies and small molecule drugs have been used clinically, high
40 cost, viral escape mutations, and potential side effects have reduced their efficacy. There is an
41 urgent need to develop a low cost treatment with wide-spectrum effect against the novel
42 variants of SARS-CoV-2.

43 Here we report a product of equine polyclonal antibodies that showed potential broad spectrum
44 neutralization effect against the major variants of SARS-CoV-2. The equine polyclonal
45 antibodies were generated by horse immunization with the receptor binding domain (RBD) of
46 SARS-CoV-2 spike protein and purified from equine serum. A high binding affinity between
47 the generated equine antibodies and the RBD was observed. Although designed against the
48 RBD of the early wild type strain sequenced in 2020, the equine antibodies also showed a
49 highly efficient neutralization capacity against the major variants of SARS-CoV-2, including
50 the recent BA.2 Omicron variant ($IC_{50} = 1.867 \mu\text{g/ml}$) in viral neutralization assay in Vero E6
51 cells using live virus cultured. The broad-spectrum neutralization capacity of the equine
52 antibodies was further confirmed using pseudovirus neutralization assay covering the major
53 SARS-CoV-2 variants including wild type, alpha, beta, delta, and omicron, showing effective
54 neutralization against all the tested strains. *Ex vivo* reconstructed human respiratory organoids
55 representing nasal, bronchial, and lung epitheliums were employed to test the treatment
56 efficacy of the equine antibodies. Antibody treatment protected the human nasal, bronchial,
57 and lung epithelial organoids against infection of the novel SARS-CoV-2 variants challenging
58 public health, the Delta and Omicron BA.2 isolates, by reducing >95% of the viral load. The
59 equine antibodies were further tested for potential side effects in a mouse model by inhalation
60 and no significant pathological feature was observed.

61 Equine antibodies, as a mature medical product, have been widely applied in the treatment of
62 infectious diseases for more than a century, which limits the potential side effects and are
63 capable of large scale production at a low cost. A cost-effective, wide-spectrum equine
64 antibody therapy effective against the major SARS-CoV-2 variants can contribute as an
65 affordable therapy to cover a large portion of the world population, and thus potentially reduce
66 the transmission and mutation of SARS-CoV-2.

67 **Key words**

68 SARS-CoV-2 therapy, receptor binding domain, equine polyclonal antibodies, airway
69 organoids

70

71 **Introduction**

72 On 24 November 2021, a novel variant strain of the severe acute respiratory syndrome
73 coronavirus 2 (SARS-CoV-2), B.1.1.529, was first reported as Omicron to the World Health
74 Organization (WHO) by South Africa(1). Soon after two days, the WHO classified B.1.1.529
75 as a variant of concern (VOC) and designated it as Omicron(2). Sub-lineages of B.1.1.529
76 including BA.1 and BA.2 emerged and spread quickly around the world, with higher
77 transmissibility and infectivity(3). BA.1 ousted the Delta variant to be the dominating variant
78 of COVID-19 and was replaced by BA.2 before long. In late April 2022, BA.2 was the most
79 dominant variant worldwide(4). Strikingly, new omicron variants are continuously emerging
80 globally. The recently appeared BA.4 and BA.5 variants display higher transmissibility and
81 neutralizing antibody evasion capability, out-competing BA.1 and BA.2(5-7). BA.4/5
82 subsequently initiated the fifth wave of COVID-19 in South Africa and have been detected in
83 more and more countries worldwide(8).

84 In these Omicron variants, there are more than 50 amino acid mutations, deletions or insertions
85 compared with ancestral virus strains, especially at the receptor binding motif in the spike
86 protein receptor binding domain (RBD), which exerted concerns of potentially increased
87 transmissibility, reduction in neutralization of spike protein by sera from vaccinated or
88 convalescent individuals, and reduced susceptibility to existing antibody treatments(2, 7).
89 Structural analysis consistently showed that mutations of Omicron variants resulted in reduced
90 affinity between the spike RBD and neutralizing antibodies(3), though the pathogenicity of
91 these Omicron variants was less than early SARS-CoV-2 strains(6). High transmissibility and
92 breakthrough infection of Omicron variants are challenging the efficacy of current therapeutics,
93 including inactivated vaccines like BNT162b2 or mRNA-1273(9-12) and monoclonal
94 antibodies like cilgavimab(8).

95 Based on the scale of the pandemic, it was estimated that single-point mutations in the large
96 SARS-CoV-2 genome would be generated every day. The pandemic situation calls urgently
97 for effective, specific, and quickly accessible drugs. Polyclonal antibodies from convalescent
98 individuals are commonly used as emergency treatments for emerging infectious diseases.
99 However, the restricted availability and the risk of bloodborne diseases have also typically
100 impeded the widespread clinical applications of the convalescent plasma(13). Equine
101 antibodies, a kind of mature and safe-to-use product with a long history, are cost-effective and
102 affordable in low-income countries where they are needed the most(14-17).

103 In this study, the RBD of SARS-CoV-2 spike protein was firstly synthesised and purified
104 followed by structural characterization via Circular dichroism spectroscopy and Fourier-
105 transform infrared spectroscopy. We then generated anti-RBD pAbs from equine serum by
106 horse immunization with obtained RBD antigens. The binding affinity of RBD antigens and
107 anti-RBD pAbs were analysed using biolayer interferometry. Several major SARS-CoV-2
108 variants in the form of both live viruses and pseudoviruses were applied in order to evaluate
109 the spectrum of antibody efficiency. In addition to viral neutralization assay using cell lines,
110 we constructed human respiratory organoids to conduct infection experiments which can better
111 reflect host responses against infection. Three different types of airway organoids, representing
112 nasal, bronchial and lung epithelium, were involved in our study to test the efficacy of the pAbs.
113 Finally, pAbs' safety was investigated using a mouse inhalation model.

114

115 **Materials and Methods**

116 **SARS-CoV-2 spike RBD protein antigen generation**

117 The SARS-CoV-2 spike protein's receptor binding domain (RBD), Arg319-Phe541 residues,
118 was cloned into a pET21a expression vector (Invitrogen) with a C-terminal 6 His tag. A single
119 colony of the construct was grown in Luria broth (LB) media for protein expression after being
120 converted into bacterial BL21 (DE3)-pLysS competent cells. A high-pressure homogenizer
121 was used to lyse the bacterial pellet. The target protein, containing in inclusion bodies, were
122 washed with urea buffer (2 M) followed by solubilizing with 8M urea-containing buffer (50
123 mM Tris, pH 9.0, 8M urea, 10 mM beta-ME). Ni²⁺ affinity chromatography and size exclusion
124 chromatography were used to purify denatured protein operating at denaturing conditions.
125 Refolding buffer (50 mM Tris, pH 9.0, 0.4 M arginine, 5 mM GSH, 0.5 mM GSSG) was then
126 prepared to perform protein refolding via fast dilution to decrease the concentration of the urea.

127

128 **Circular dichroism spectroscopy**

129 The secondary structure of the generated RBD was measured by the far-UV circular dichroism
130 (CD) spectroscopy, using a Chirascan spectropolarimeter. Refolded RBD was dialyzed into PB
131 buffer (pH 7.4) followed by diluting to a concentration of 0.2 mg/ml for CD measurement. The
132 spectrum was recorded between 260 nm and 190 nm at 20 °C. The spectra represented an
133 average of three individual scans and were corrected for absorbance caused by the buffer. A
134 quartz cuvette with a 0.1 cm path length was used for the measurement. The data was processed
135 and smoothed via the Graphpad Prism 8.0.1 software.

136

137 **Fourier-transform infrared spectroscopy**

138 The Fourier-transform infrared (FTIR) spectrometer (Bruker Vertex 70v) coupled with a
139 diamond ATR accessory was used to measure the infrared spectra of RBD using the attenuated
140 total reflectance (ATR) method. Atmospheric effects were eliminated by collecting spectrum
141 without a sample prior to the test. 10 mg/ml RBD protein in PBS buffer or PBS buffer alone
142 were positioned onto the diamond crystal surface. After drying under a stream of nitrogen, the
143 deposited film served as the sample and background respectively. Every spectrum is typically
144 recorded with 256 scans at a resolution of 2 cm⁻¹.

145

146 **Immunization of horses with RBD**

147 Anti-RBD antibodies were generated by immunizing healthy horses with no detectable
148 antibodies against SARS-CoV-2. The obtained RBD antigens were sterilized by ultra-filtration.
149 Horses were immunized and collected for antisera. The horse sera before immunization
150 were also collected for negative controls of antibody evaluation. The titers of sera were
151 tested by an ELISA assay using cPass™ SARS-CoV-2 Neutralization Antibody Detection Kit
152 following standard procedure(18).

153

154 **Biolayer interferometry (BLI) analysis of RBD and antibody binding affinity**

155 Anti-RBD-pAbs binding affinities towards the RBD antigen was measured by BLI on an Octet
156 Red 96 instrument (ForteBio, USA) using Ni-NTA biosensors at 30°C with shaking at
157 1000 rpm. A 60s baseline measurement in kinetics buffer (PBS, 0.02% Tween 20) was
158 conducted firstly followed by loading of RBD antigens (500 nM) for 180 s. Then a second
159 baseline measurement was performed in kinetics buffer for 180 s. 180 s association and 300 s
160 dissociation of anti-RBD pAbs were conducted in different pAbs solutions and kinetics buffer
161 respectively. Results were analyzed by ForteBio Data Analysis software (10.0.3.1). The K_D
162 value of RBD or Tn-RBD binding affinity to pAb was calculated from the binding curves based
163 on the global fit to a 1:1 Langmuir binding model with an R^2 value of ≥ 0.95 . The kinetically
164 derived affinities were calculated as $K_D = K_{dis}/K_{on}$.

165

166 **Cells and viruses**

167 Vero E6 cells (African green monkey kidney cell, ATCC CCL-81) were cultured in complete
168 culture media (Dulbecco's Modified Eagle Medium (DMEM; Thermo Fisher Scientific, USA)
169 supplemented with 10% fetal bovine serum (FBS) and penicillin (100 U/ml)–streptomycin
170 (100 mg/ml)) at 37°C under 5% CO₂. SARS-CoV-2/shenzhen/02/2020 (WT), SARS-CoV-
171 2/shenzhen/09/2022(Delta), SARS-CoV-2/shenzhen/08/2022(Omicron BA.1) and SARS-
172 CoV-2/shenzhen/13/2022(Omicron BA.2) were isolated from throat swabs from patients tested
173 positive for SARS-CoV-2. All strains were confirmed by sequencing. Standard plaque assay
174 on Vero E6 cells were conducted for determining virus titers and the virus stocks were stored
175 in aliquots at -80°C until required.

176

177 **Neutralization assay**

178 Virus:

179 20,000 Vero E6 cells were seeded in each well of a 96-well plate with 100 µl culture media
180 and cultured at 37°C and 5% CO₂. After overnight culture, cells were then treated with 100 µl
181 virus/antibody mixture solution and incubated for another 1 h. Virus solution was prepared by
182 diluting in culture media allowing the multiplicity of infection (MOI) reach 0.01.
183 Virus/antibody mixture solution was obtained by mixing 60 µl anti-RBD-pAbs solution at
184 serial-diluted concentrations with culture media and 60 µl virus solution. The mixture was
185 incubated at 37°C and 5% CO₂ for 1h prior to cell infection. The infection media was discarded
186 after infection and the cells were washed with 200 µl PBS twice followed by incubating with
187 carboxymethyl cellulose containing DMEM culture media (#C4888, Sigma). SARS-CoV-2 NP
188 protein in the infected cells was stained for standard ELISpot assay and analyzed by CTL
189 Immunospot analyzer. Infection solution containing pure virus solution (i.e. no antibody) or
190 pure culture media solution were considered virus control and blank control, respectively.
191 Neutralization ratio was determined as:

$$192 \text{ Neutralization\%} = \left(1 - \frac{\text{Sample-Blank control}}{\text{Virus control-Blank control}}\right) \times 100\%$$

193

194 Pseudovirus:

195 The pseudovirus including SARS-CoV-2 WT, Delta, Omicron, Beta and Alpha were purchased
196 from Vazyme. 18,000 293T-ACE2 cells were seeded in each well of a 96-well plate with 100
197 μ L culture media. After overnight culture at 37°C and 5% CO₂, 293T-ACE2 cells were treated
198 with 100 μ l pseudovirus/antibody mixture solution and cultured for another 48 h. Pseudovirus
199 solution was prepared by diluting pseudovirus with culture media to a final concentration of
200 1.3×10^4 TCID₅₀/ml. 60 μ l anti-RBD-pAb solution were prepared at serial-diluted
201 concentrations in culture media and then mixed with 60 μ l pseudovirus solution. The mixture
202 was incubated at 37°C and 5% CO₂ for 1h prior to cell infection. Neutralizing activity was
203 determined via bioluminescence detection using a microplate reader following the
204 manufacturer's protocol (Bio-Lite Luciferase Assay System, Vazyme). Briefly, 96-well plates
205 were equilibrated to room temperature first. The culture media was discarded, followed by
206 gentle washing with 100 μ L PBS. 100 μ l luciferase substrate solution was then added and the
207 bioluminescence was measured after incubating the plate for 10 min at room temperature.

208

209 **Construction of 2-D airway organoids**

210 Airway epithelial progenitor cells for 2-D airway organoid culture were derived from patients'
211 surplus nasal, bronchial or lung biopsy, respectively. The obtained biopsy samples were rinsed
212 with cold DPBS and minced into small pieces for subsequent Dispase I (Stemcell Technologie,
213 CA) dissolving. The harvested cells were cultured in PneumaCult™-Ex Plus Medium
214 (Stemcell Technologie, CA) and then co-cultured with NIH-3T3 feeder cells. When confluent,
215 the cells were transferred to transwells with 0.4 μ m pores (Corning transwell 3470) and
216 cultured at 37°C under 5% CO₂. The cells were cultured on an air-liquid interface (ALI) for
217 differentiation in culture media (PneumaCult ALI media, STEMCELL Technologies, Canada)
218 to allow the progenitor cells to differentiate into a mucociliary airway epithelium. Experimental
219 design was reviewed and approved by the ethics committee of the Seventh Affiliated Hospital
220 of Sun Yat-sen University (KY-2021-075-02). Written informed consents were signed by the
221 involved patients as well.

222

223 **SARS-CoV-2 infection of 2-D airway organoids**

224 The infection experiments were performed on day 21 of differentiation. 50 μ l media containing
225 10,000 plaque-forming units (PFUs) SARS-CoV-2 was added into the inserts of the transwell
226 plate and incubated for 1 h. The infected organoids in the inserts were then transferred to a new
227 plate after washing for 3 times with PBS. 500 μ l serum-free growth medium (05001, 296
228 STEMCELL Technologies, CA, USA) was added and incubated. 150 μ l PBS was added into
229 the transwell's apical compartment before samples were collected for analysis. Cells and
230 samples, including the PBS wash, were all collected.

231

232 **Anti-RBD pAbs intake *in vivo* model**

233 The animal study was approved by Institutional Animal Care and Use Committee, Shenzhen
234 Institute of Advanced Technology, Chinese Academy of Sciences (SIATACUC-YYS-LL-

235 A0550). Anti-RBD pAbs or saline control were inhaled by 8 week old C57 mice intranasally.
236 Lung samples were collected on day 3 after inhalation for H&E staining.

237

238 **Quantification of Viral Gene Expression by qPCR**

239 RNA was extracted from PBS wash described above using TRIzol™ (Invitrogen™, Thermo
240 Fisher Scientific). The extracted RNAs were reversed transcribed into cDNA using a
241 PrimeScrip RT reagent kit (Takara, Japan) and quantified using Coronavirus 2019-nCoV
242 nucleic acid detection kit (fluorescent PCR method) (BioGerm, Shanghai, China) following
243 manufacture's protocol.

244

245 **Results**

246 The applied methodologies for this study were summarized in Figure 1 schematically. Briefly,
247 recombinant SARS-CoV-2 spike RBD protein antigens were expressed in *E.coli* cells and then
248 purified chromatographically. Horses were then immunized with the obtained RBD protein
249 antigen to generate the equine anti-RBD serum. The anti-RBD pAbs were isolated from the
250 serum and further sterilized via filtration. Its efficacy were evaluated against SARS-CoV-2 and
251 several variants in 2-D airway organoid models including nasal, bronchial and lung. All of the
252 organoids were infected with live viruses (SARS-CoV-2 WT, Delta, Omicron BA.1 and BA.2)
253 and treated separately with mock control and equine anti-RBD pAbs. The virus content in the
254 topical release from each group were measure by qPCR thereby evaluating the treatment effects.
255 Besides, *in vivo* experiments were also conducted for pAbs safety evaluation (**Figure 1a**).

256

257 **Characterization of receptor-binding domain antigen and binding affinity to pAbs**

258 CD spectroscopy and FTIR spectroscopy were used to structurally characterize the RBD
259 antigens' structure. As shown in **Figure 1b**, the CD spectrum of *E.coli* produced RBD showed
260 a single minimum at 207 nm, suggesting a characteristic of β -sheet structure. Besides, a
261 maximum around 230 nm was observed, suggesting the contribution of aromatic residues. This
262 is similar to that observed for RBD antigens produced from mammalian or yeast cells(19). The
263 FTIR spectrum (**Figure 1c**) displayed the characteristic peaks at 1614 cm^{-1} (Amide I, C=O
264 vibration), 1467 cm^{-1} (Amide II, N-H stretching) and 2971 cm^{-1} (C-H stretching). Besides,
265 it also showed small peaks around $1100\text{ to }1300\text{ cm}^{-1}$ for Amide III vibration. As compared
266 with the native β -sheet proteins, which typically peak from $1630\text{ to }1643\text{ cm}^{-1}$ for amide I, the
267 shift may be caused by more extended β -sheets or unordered structures.

268 RBD antigen binding affinity to pAbs were measured by BLI. For all the binding curves, the
269 values increased with the associating time and showed little change curing dissociating process
270 (**Figure 1d**). K_{on} and K_{off} , representing the rate constant of association and dissociation
271 respectively, were found the same among all the tested concentrations ($1.24E4\text{ Ms}^{-1}$ for K_{on}
272 and $2.56E-4\text{ s}^{-1}$ for K_{off}). The results showed that RBD binds to pAb efficiently with a K_D value
273 of $20.6 \pm 0.59\text{ nM}$, indicating a good binding affinity between RBD and equine pAbs.

274

275 **Neutralization activity assessment of anti-RBD pAbs**

276 To evaluate the neutralization activity of the anti-RBD pAbs, both virus and pseudovirus were
277 employed in our study. The neutralizing activity of pAbs towards SARS-CoV-2 virus and their
278 mutants were tested using Vero E6 cells and determined by the content of virus nucleocapsid
279 in cells after infection. The IC_{50} values of pAbs towards SARS-CoV-2 WT, Delta, BA.1 and
280 BA.2 mutants were 0.491, 0.254, 0.578 and 1.867 $\mu\text{g/ml}$, respectively (**Figure 2a**). As to
281 pseudovirus assay, the neutralization activity was assessed using 293T-ACE2 cells by
282 measuring the relative luciferase expression after infection. The IC_{50} values of pAbs against
283 SARS-Cov-2 WT, Delta, Omicron, Beta and Alpha were 0.116, 2.640, 1.190, 13.544 and 3.999
284 $\mu\text{g/ml}$ respectively. The results suggest our pAbs have a broad-spectrum neutralization capacity
285 towards various SARS-CoV-2 variants in both virus and pseudovirus assays.

286 **2-D airway organoid construction and SARS-CoV-2 infection**

287 Different types of 2-D airway organoids including nasal, bronchial and lung epitheliums were
288 constructed to represent SARS-CoV-2 airway infection. Using nasal organoids as an example,
289 the primary progenitor cells from nasal biopsy were planted in transwell inserts and
290 differentiated in ALI as described in methods section. A pseudostratified epithelium containing
291 goblet cells and ciliated columnar cells were developed and capable of generating mucus. As
292 shown in **Figure 3a**, immunofluorescent staining revealed the apical cells containing both
293 goblet cells (labeled with MUC5AC in red) and ciliated cells (labeled with Ac- α -tubulin in
294 green), indicating the nasal progenitor cells were well differentiated to form a nasal epithelium.
295 Together with the H&E staining (**Figure 3b**) which showed well-organized structures and high
296 similarities compared with nasal biopsy reported in the literatures(20-22), the nasal organoids
297 were confirmed as successfully constructed. The 2-D airway organoids were then applied in
298 the infection model as a testing platform for the neutralization effect of the antibodies. As
299 shown in **Figure 3c** and **3d**, organoids with mock-infection (**Figure 3c**) showed no spike
300 protein expression, while SARS-CoV-2 spike labeled in green were observed in the apical cells
301 (**Figure 3d**) suggested the feasibility of this infection model. We further extended this model
302 for bronchial and lung epitheliums.

303 **Anti-RBD-pAb efficacy and safety assessment**

304 The anti-RBD-pAb efficacy was tested using the organoid infection models constructed. A
305 typical SARS-CoV-2 qPCR kit was used to quantify the topical release of the virus. Delta and
306 BA.2 viral strains were used to infect the organoids constructed to respresent nasal, bronchial
307 and lung epitheliums. As shown in **Figure 4a**, a significant reduction in the ORF1ab and N
308 RNA content were observed in the anti-RBD pAb-treated groups (Inf+Ab) among all organoid
309 models for SARS-CoV-2 infection compared with their non-treated infection counterparts.
310 **Figure 4b** illustrated similar trends for BA.2-infected organoids that the virus content was
311 decreased in pAb-treated groups. We then applied mouse inhalation model to evaluate the
312 safety of our pAbs. As shown in **Figure 4c** and **4d**, H&E staining of lung sections after either
313 saline or anti-RBD pAbs inhalation showed no significant immune cell infiltration in the mouse
314 lungs, demonstrating that the pAbs did not induce significant immune responses in the mouse
315 model.

316

317

318 Discussion

319 COVID-19 caused by SARS-CoV-2 has emerged worldwide as an unprecedented public health
320 emergency for more than 2 years. Vaccine development has been considered as the best long-
321 term solution to this pandemic. To date, many types of SARS-CoV-2 vaccines have been
322 licensed and administered(23). However, SARS-CoV-2 still poses significant health challenges
323 globally even after boost doses have been required for nearly a year. This is mainly due to the
324 constant emerge of new variants of SARS-CoV-2, the uneven accessibility of vaccines,
325 especially for developing countries, and the effectiveness and side effect concerns of vaccines
326 among the pregnant, the elderly and the immunocompromised populations. This highlights the
327 critical needs for a broad-spectrum treatment capable of large scale production at relatively low
328 cost(24). With decades of experience on equine antibodies production, we conducted SARS-
329 CoV-2 antibody production via horse immunization with the RBD antigens of the SARS-CoV-
330 2 spike protein followed by antibody purification. Our obtained anti-RBD pAbs were then
331 tested against the major variants of SARS-CoV-2 and showed potent neutralization capability
332 against both live virus and pseudovirus (**Figure 2**). Their excellent efficacy were also
333 demonstrated on several respiratory organoid SARS-CoV-2 infection models including nasal,
334 bronchial and lung organoids, showing significant blockage of viral infection and reduction of
335 viral replication upon treatment by equine polyclonal antibodies (**Figure 4**). Our study
336 demonstrated equine anti-RBD pAbs had great potential as a broad-spectrum and cost-effective
337 drug. The manufacture of equine antibody drugs has already been well established, with mature
338 production lines and production processes, making side effects manageable. Besides, the
339 overall development allowing mass production of new equine antibodies within 6 months
340 enables the quick adaption towards new variants when needed, further making them a
341 promising solution for this and future possible pandemics.

342 In terms of safety and effectiveness for long term usage, equine products had showed their
343 advantages over vaccines and small molecular drugs in several aspects including drug
344 resistance and evasion by novel variants, hepatotoxicity and nephrotoxicity. In late 2021,
345 multiple new variants of SARS-CoV-2, including the alpha, beta, delta and omicron variants,
346 have drawn great concern due to their enhanced transmissibility, virulence and the potential of
347 immune evasion from the host defense built by both vaccinations and previous infections of
348 SARS-CoV-2. More lines of evidence have demonstrated the decreased protection from some
349 vaccine products towards these mutants(25-28). The hindered accessibility to COVID-19
350 vaccines in low-income countries caused differences in the levels of inoculation, which could
351 also lead to virus mutations and new variants(29). As to small molecule drugs, their liver and
352 kidney toxicity, relatively long development timeline and drug resistance issues were the
353 general concerns raised. Given the past history of small molecular drug development for
354 influenza virus, the continuous evolvement of influenza virus caused rapid emergence of
355 resistance to existing drugs, particularly to adamantanes, followed by oseltamivir, highlighting
356 the constant requirements for new drug development(30). It could be anticipated that the widely
357 disseminated SARS-CoV-2 virus will also develop drug resistance problems within a relatively
358 short time frame due to its wide spread globally. Equine antibodies, as mature antibody
359 therapeutics, can overcome these limitations. Their safety has been recognized for ages by
360 World Health Organization over several widespread diseases(31). In this paper, our results
361 showed the possibilities of using horse immunization to generate anti-RBD pAbs with excellent
362 neutralization activities against several wide spread SARS-CoV-2 variants including Delta,

363 BA.1 and BA.2, on top of WT. Besides, the neutralization effects were also observed using
364 nasal, bronchial and lung epithelial organoid infection models that significant reduction of virus
365 content were shown among all the tested organoids. Our *in vivo* study by a mice inhalation
366 model found no significant differences in lung tissue morphology between a saline control and
367 the antibody treatment (**Figure 4**), confirming on the safety of the anti-RBD pAbs.

368 Equine antibodies are cost-effective therapeutic products compared to other antibodies. Using
369 polyclonal antibodies derived from horses for the treatment of diseases like rabies, tetanus,
370 diphtheria etc. is a well-known and easily scalable technology owing a history of over a century
371 across the world(32-37). In our study, after horse immunization, large amounts of sera can be
372 collected monthly in a repeated manner to generate high titers of neutralizing antibodies. The
373 harvested antibodies showed high binding affinity towards RBD antigens and potent
374 neutralization activity towards both live virus and pseudovirus of several major variants of
375 SARS-CoV-2. Since equine relevant products are routinely produced in developing countries,
376 it could be easily produced in many parts of the world to ensure the accessibility of effective
377 COVID-19 treatments especially for low-income population.

378 The proposed administration routine of our equine anti-RBD pAbs includes both inhalation
379 and injection in future clinical applications. The inhalation method exhibit various advantages
380 on prophylactic and therapeutic applications(38). For example, inhalation can block the
381 transmission route among individuals by attaching the antibodies on the respiratory tract
382 surfaces, which can prevent virus invasion into the airway cells and also prevent the virus from
383 being coughed up by the patient. Besides, there are less side effects for the inhalation
384 administration due to its topical medication in the airway. Considering neutralizing antibodies
385 should block the internalization of the virus, early stage and asymptomatic patients could also
386 benefit to prevent severe illness and viral transmission, which is enabled by the low cost and
387 high safety of the equine pAbs.

388 The possible reason of our equine anti-RBD pAbs having broad spectrum neutralization effect
389 towards the major SARS-CoV-2 variants is potentially due to the intrinsic complex immune
390 responses in horses tending to develop broad spectrum avidity than monoclonal antibodies for
391 their cognate antigens(39). pAbs recognize a vast array of epitopes, reducing the risk of viral
392 escape mutations. In addition, healthy horses generally had better tolerance towards the side
393 effects of immunization by antigens than human beings, especially for the elderly, pregnant
394 and immunocompromised population. We believe with the advances in the vaccine technology
395 development such as nucleic acid vaccines, the production of equine antibodies against possible
396 new mutant strains using equine immunization by new forms of vaccine-like products can be
397 further accelerated. This low-cost, broad-spectrum and highly productive equine antibodies
398 could be beneficial to a broader population including people who respond inefficiently to
399 vaccines and people who cannot afford expensive medications.

400

401

402 **References:**

- 403 1. SARS-CoV-2 B.1.1.529 (Omicron) Variant - United States, December 1-8, 2021. *MMWR Morb*
404 *Mortal Wkly Rep.* 2021;70(50):1731-4.
- 405 2. Wong S-C, Au AK-W, Chen H, Yuen LL-H, Li X, Lung DC, et al. Transmission of Omicron
406 (B.1.1.529) - SARS-CoV-2 Variant of Concern in a designated quarantine hotel for travelers: a challenge
407 of elimination strategy of COVID-19. *The Lancet Regional Health - Western Pacific.* 2022;18:100360.
- 408 3. Kannan SR, Spratt AN, Sharma K, Chand HS, Byrareddy SN, Singh K. Omicron SARS-CoV-2
409 variant: Unique features and their impact on pre-existing antibodies. *Journal of Autoimmunity.*
410 2022;126:102779.
- 411 4. Mohapatra RK, Kandi V, Verma S, Dhama K. Challenges of the Omicron (B.1.1.529) Variant and
412 Its Lineages: A Global Perspective. *ChemBioChem.* 2022;23(9):e202200059.
- 413 5. Cao Y, Yisimayi A, Jian F, Song W, Xiao T, Wang L, et al. BA.2.12.1, BA.4 and BA.5 escape
414 antibodies elicited by Omicron infection. *Nature.* 2022.
- 415 6. Uraki R, Kiso M, Iida S, Imai M, Takashita E, Kuroda M, et al. Characterization and antiviral
416 susceptibility of SARS-CoV-2 Omicron BA.2. *Nature.* 2022;607(7917):119-27.
- 417 7. Lu L, Mok BW-Y, Chen L-L, Chan JM-C, Tsang OT-Y, Lam BH-S, et al. Neutralization of Severe
418 Acute Respiratory Syndrome Coronavirus 2 Omicron Variant by Sera From BNT162b2 or CoronaVac
419 Vaccine Recipients. *Clinical Infectious Diseases.* 2021.
- 420 8. Mohapatra RK, Kandi V, Sarangi AK, Verma S, Tuli HS, Chakraborty S, et al. The recently
421 emerged BA.4 and BA.5 lineages of Omicron and their global health concerns amid the ongoing wave
422 of COVID-19 pandemic – Correspondence. *International Journal of Surgery.* 2022;103:106698.
- 423 9. Ai J, Zhang H, Zhang Y, Lin K, Zhang Y, Wu J, et al. Omicron variant showed lower neutralizing
424 sensitivity than other SARS-CoV-2 variants to immune sera elicited by vaccines after boost. *Emerg*
425 *Microbes Infect.* 2022;11(1):337-43.
- 426 10. Cele S, Jackson L, Khoury DS, Khan K, Moyo-Gwete T, Tegally H, et al. Omicron extensively but
427 incompletely escapes Pfizer BNT162b2 neutralization. *Nature.* 2022;602(7898):654-6.
- 428 11. Wang Y, Zhan W, Liu J, Wang Y, Zhang X, Zhang M, et al. A broadly neutralizing antibody against
429 SARS-CoV-2 Omicron variant infection exhibiting a novel trimer dimer conformation in spike protein
430 binding. *Cell Research.* 2022.
- 431 12. Hachmann NP, Miller J, Collier A-RY, Ventura JD, Yu J, Rowe M, et al. Neutralization Escape by
432 SARS-CoV-2 Omicron Subvariants BA.2.12.1, BA.4, and BA.5. *N Engl J Med.* 2022;387(1):86-8.
- 433 13. Pan X, Zhou P, Fan T, Wu Y, Zhang J, Shi X, et al. Immunoglobulin fragment F(ab')₂ against RBD
434 potentially neutralizes SARS-CoV-2 in vitro. *Antiviral Research.* 2020;182:104868.
- 435 14. Heterologous Antisera and Antivenins Are Essential Biologicals: Perspectives on a Worldwide
436 Crisis. *Annals of Internal Medicine.* 1996;125(3):233-6.
- 437 15. Bal C, Herbreteau CH, Buchy P, Rith S, Zaid M, Kristanto W, et al. Safety, potential efficacy, and
438 pharmacokinetics of specific polyclonal immunoglobulin F(ab')₂ fragments against avian influenza A
439 (H5N1) in healthy volunteers: a single-centre, randomised, double-blind, placebo-controlled, phase 1
440 study. *The Lancet Infectious Diseases.* 2015;15(3):285-92.
- 441 16. Lu J-h, Guo Z-m, Han W-y, Wang G-l, Zhang D-m, Wang Y-f, et al. Preparation and development
442 of equine hyperimmune globulin F(ab')₂ against severe acute respiratory syndrome coronavirus. *Acta*
443 *Pharmacologica Sinica.* 2005;26(12):1479-84.
- 444 17. Pan X, Wu Y, Wang W, Zhang L, Xiao G. Development of horse neutralizing immunoglobulin
445 and immunoglobulin fragments against Junin virus. *Antiviral Research.* 2020;174:104666.
- 446 18. Tan CW, Chia WN, Qin X, Liu P, Chen MIC, Tiu C, et al. A SARS-CoV-2 surrogate virus
447 neutralization test based on antibody-mediated blockage of ACE2–spike protein–protein interaction.
448 *Nature Biotechnology.* 2020;38(9):1073-8.
- 449 19. Arbeitman CR, Auge G, Blaustein M, Bredeston L, Corapi ES, Craig PO, et al. Structural and
450 functional comparison of SARS-CoV-2-spike receptor binding domain produced in *Pichia pastoris* and
451 mammalian cells. *Scientific Reports.* 2020;10(1):21779.

- 452 20. He Y, Qu J, Wei L, Liao S, Zheng N, Liu Y, et al. Generation and Effect Testing of a SARS-CoV-2
453 RBD-Targeted Polyclonal Therapeutic Antibody Based on a 2-D Airway Organoid Screening System.
454 *Front Immunol.* 2021;12:689065.
- 455 21. Tong L, Xiao X, Li M, Fang S, Ma E, Yu X, et al. A glucose-like metabolite deficient in diabetes
456 inhibits cellular entry of SARS-CoV-2. *Nat Metab.* 2022;4(5):547-58.
- 457 22. Xu G, Li Y, Zhang S, Peng H, Wang Y, Li D, et al. SARS-CoV-2 promotes RIPK1 activation to
458 facilitate viral propagation. *Cell Research.* 2021;31(12):1230-43.
- 459 23. Krammer F. SARS-CoV-2 vaccines in development. *Nature.* 2020;586(7830):516-27.
- 460 24. Alkandari D, Herbert JA, Alkhalaf MA, Yates C, Panagiotou S. SARS-CoV-2 vaccines: fast track
461 versus efficacy. *The Lancet Microbe.* 2021;2(3):e89-e90.
- 462 25. Boehm E, Kronig I, Neher RA, Eckerle I, Vetter P, Kaiser L. Novel SARS-CoV-2 variants: the
463 pandemics within the pandemic. *Clin Microbiol Infect.* 2021;27(8):1109-17.
- 464 26. Zhou D, Dejnirattisai W, Supasa P, Liu C, Mentzer AJ, Ginn HM, et al. Evidence of escape of
465 SARS-CoV-2 variant B.1.351 from natural and vaccine-induced sera. *Cell.* 2021;184(9).
- 466 27. Madhi SA, Baillie V, Cutland CL, Voysey M, Koen AL, Fairlie L, et al. Efficacy of the ChAdOx1
467 nCoV-19 Covid-19 Vaccine against the B.1.351 Variant. *N Engl J Med.* 2021;384(20):1885-98.
- 468 28. Edara V-V, Pinsky BA, Suthar MS, Lai L, Davis-Gardner ME, Floyd K, et al. Infection and Vaccine-
469 Induced Neutralizing-Antibody Responses to the SARS-CoV-2 B.1.617 Variants. *N Engl J Med.*
470 2021;385(7):664-6.
- 471 29. Acharya KP, Ghimire TR, Subramanya SH. Access to and equitable distribution of COVID-19
472 vaccine in low-income countries. *npj Vaccines.* 2021;6(1):54.
- 473 30. Shen Z, Lou K, Wang W. New small-molecule drug design strategies for fighting resistant
474 influenza A. *Acta Pharm Sin B.* 2015;5(5):419-30.
- 475 31. Pakdemirli A, Çalişkan E, Hacıoğlu S, Danyer E, Kardoğan Ö, Ergün Kurt Z, et al. History repeats
476 itself: horse originated hyperimmune sera production against SARS CoV-2. *Turk J Med Sci.*
477 2021;51(5):2263-73.
- 478 32. Watt G, Kantipong P, Jongsakul K, de Souza M, Burnouf T. Passive transfer of scrub typhus
479 plasma to patients with AIDS: a descriptive clinical study. *QJM.* 2001;94(11):599-607.
- 480 33. Savoldo B, Goss J, Liu Z, Huls MH, Doster S, Gee AP, et al. Generation of autologous Epstein-
481 Barr virus-specific cytotoxic T cells for adoptive immunotherapy in solid organ transplant recipients.
482 *Transplantation.* 2001;72(6):1078-86.
- 483 34. Chiba T, Yokosuka O, Goto S, Fukai K, Imazeki F, Shishido H, et al. Successful clearance of
484 hepatitis B virus after allogeneic stem cell transplantation: beneficial combination of adoptive
485 immunity transfer and lamivudine. *Eur J Haematol.* 2003;71(3):220-3.
- 486 35. Ferrantelli F, Rasmussen RA, Hofmann-Lehmann R, Xu W, McClure HM, Ruprecht RM. Do not
487 underestimate the power of antibodies—lessons from adoptive transfer of antibodies against HIV.
488 *Vaccine.* 2002;20:A61-A5.
- 489 36. Dahmen U, Dirsch O, Li J, Fiedle M, Lu M, Rispeter K, et al. Adoptive transfer of immunity: a
490 new strategy to interfere with severe hepatitis virus reinfection after woodchuck liver transplantation.
491 *Transplantation.* 2004;77(7):965-72.
- 492 37. Xu Y, Jia Z, Zhou L, Wang L, Li J, Liang Y, et al. Evaluation of the safety, immunogenicity and
493 pharmacokinetics of equine anti-SARS-CoV F(ab')₂ in macaque. *International Immunopharmacology.*
494 2007;7(13):1834-40.
- 495 38. Jeyananthan V, Afkhami S, D'Agostino MR, Zganiacz A, Feng X, Miller MS, et al. Differential
496 Biodistribution of Adenoviral-Vectored Vaccine Following Intranasal and Endotracheal Deliveries
497 Leads to Different Immune Outcomes. *Front Immunol.* 2022;13:860399.
- 498 39. Zylberman V, Sanguineti S, Pontoriero AV, Higa SV, Cerutti ML, Morrone Seijo SM, et al.
499 Development of a hyperimmune equine serum therapy for COVID-19 in Argentina. *Medicina (B Aires).*
500 2020;80 Suppl 3:1-6.

501
502

503 **Acknowledgments**

504 The study was supported by the National Natural Science Foundation of China (81900071),
505 the Natural Science Foundation of Guangdong Province of China (2021A1515010004),
506 Shenzhen Science and Technology Program (JCYJ20190809143601759) and SUSTech
507 Starting-up Research Grant (Y01416133).

508 Figure 1A was created using BioRender.com.

509

510 **Author Contributions**

511 Study design: LL, PW, ZX, JQ; Experiments: SML, YJH, JQ, YZL, KLZ, JHC, YJ, CKS, CJ,
512 GXL, SL, YPF, ZQL, SSF, YQH, XSZ, CLW, RLZ; Data analysis: SML, YJH, YS, JQ, LL;
513 Manuscript: SML, YS, LL.

514

515 **Declaration of Competing Interests**

516 The authors declare no competing interests for the publication of the work.

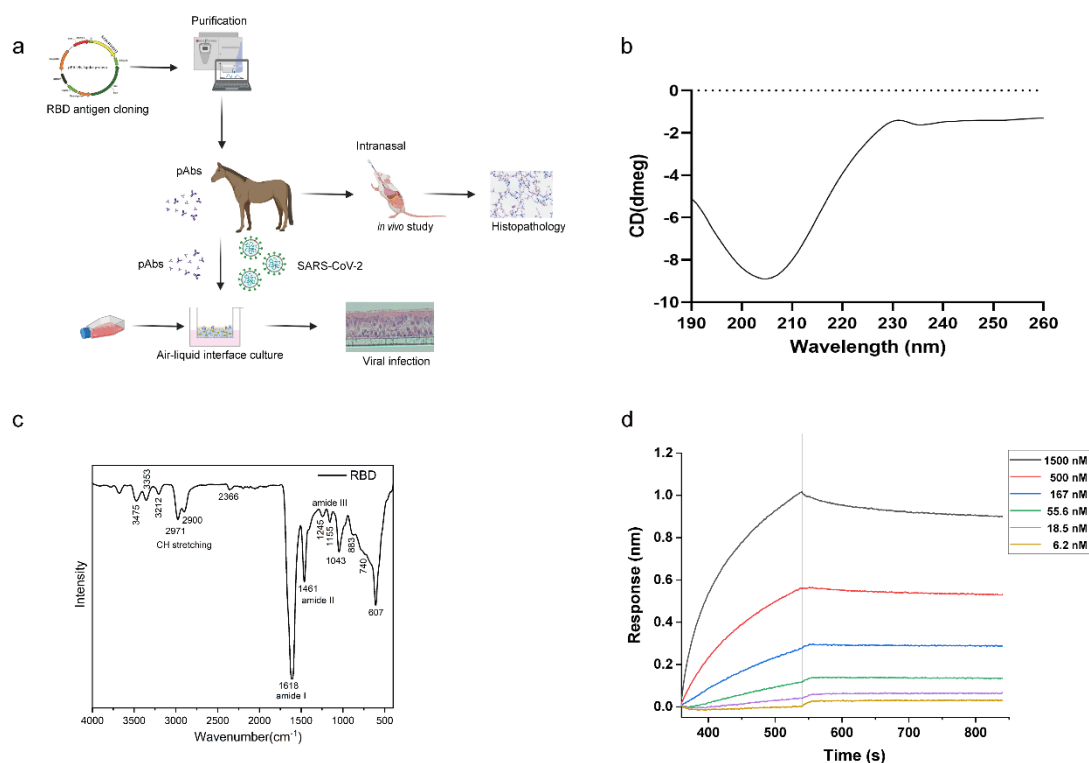
517

518 **Conflicts of Interests**

519 The authors Yue Jing, Clifton Kwang-Fu Shen, Chong Ji, Xusheng Zhao, and Guxun Luo are
520 currently employed by Jiangxi Institute of Biological Products Co. Ltd., Jiangxi, China, and
521 Jiangxi Institute of Biological Products Shenzhen R&D Center Co. Ltd., Shenzhen, China. The
522 remaining authors declare that the research was conducted in the absence of any commercial
523 or financial relationships that could be construed as a potential conflict of interests.

524 **Figure legends:**

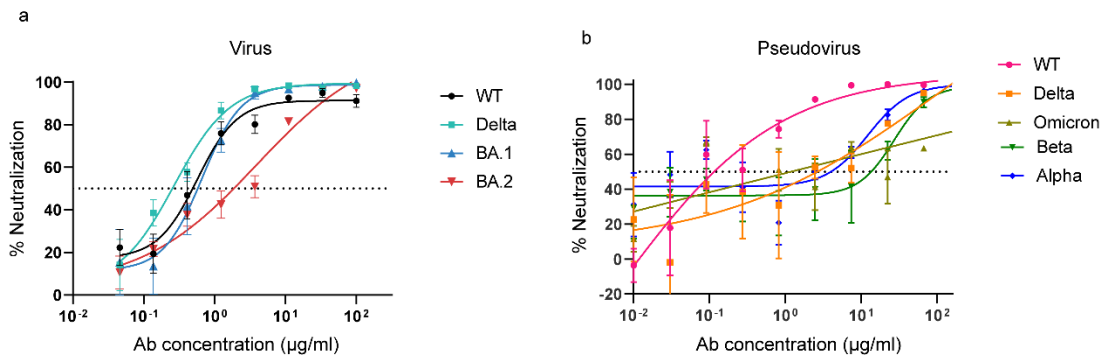
525 **Figure 1:**



526

527 **Figure 1.** Overview of the study design (a) and RBD characterization (b, c). (a) The RBD
528 antigen was firstly cloned into a vector and purified chromatographically. Then the anti-RBD
529 polyclonal antibodies (pAbs) extracted from horse serum were tested both *in vitro* and *in*
530 *in vivo*. The binding efficacy of antibodies was tested. 2-D airway organoids including nasal,
531 bronchial and lung epitheliums constructed by differentiation in air liquid interphase (ALI)
532 were infected by SARS-CoV-2 and used to evaluate the efficacy of the anti-RBD pAbs.
533 Finally, the anti-RBD pAbs' safety was tested *in vivo*. The obtained RBD antigen were
534 characterized via CD spectroscopy (b) and FTIR spectroscopy (c) recording the spectrum
535 from 190-260nm and 400-4000nm respectively. (d) The binding curves were generated from
536 basic kinetics analysis of 1500nM, 500nM, 167nM, 55.6nM, 18.5nM and 6.2 nM anti-RBD-
537 pAbs. The association were performed for 550s followed by dissociation in PBS.

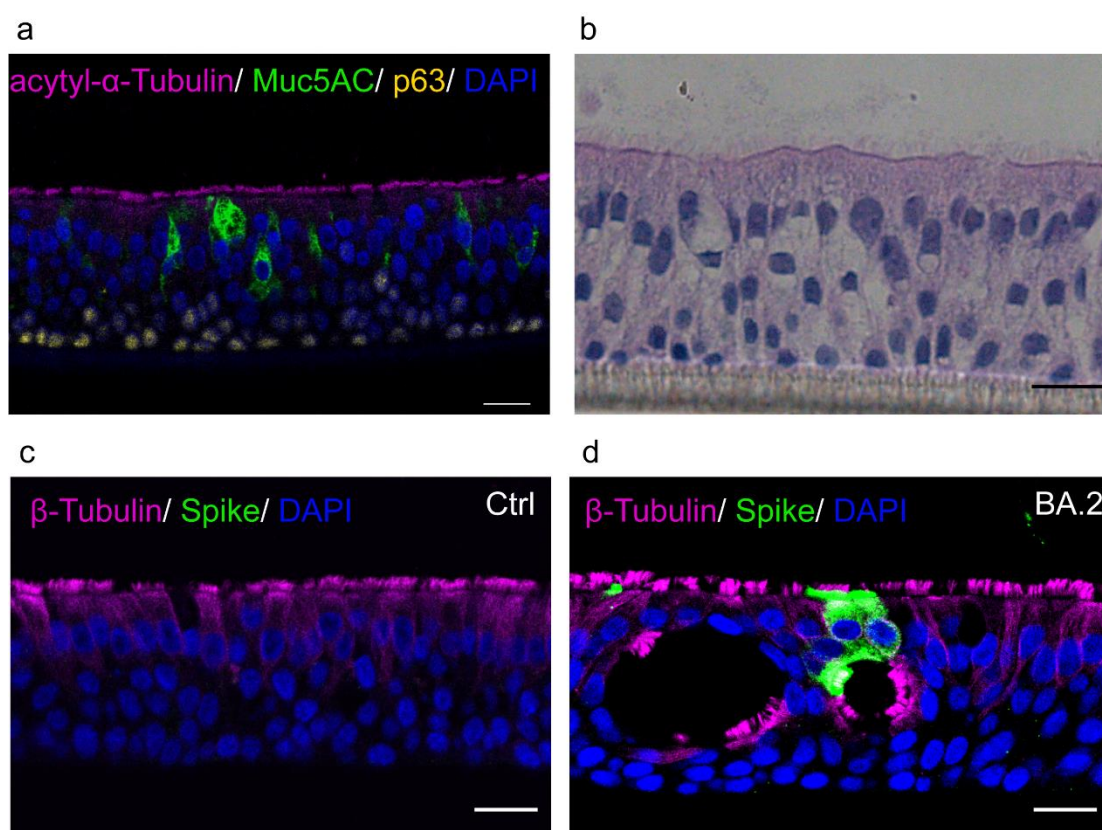
538 **Figure 2:**



539

540 **Figure 2.** Anti-RBD-pAbs demonstrate potent neutralizing activity towards live virus (SARS-
541 CoV-2 WT, Delta, Omicron BA.1 and BA.2 strains) (a) and pseudovirus (SARS-CoV-2 WT,
542 Delta, Omicron, Beta and Alpha) (b). IC₅₀ was determined as the concentration of anti-RBD-
543 pAbs at which 50% of neutralization is reached.

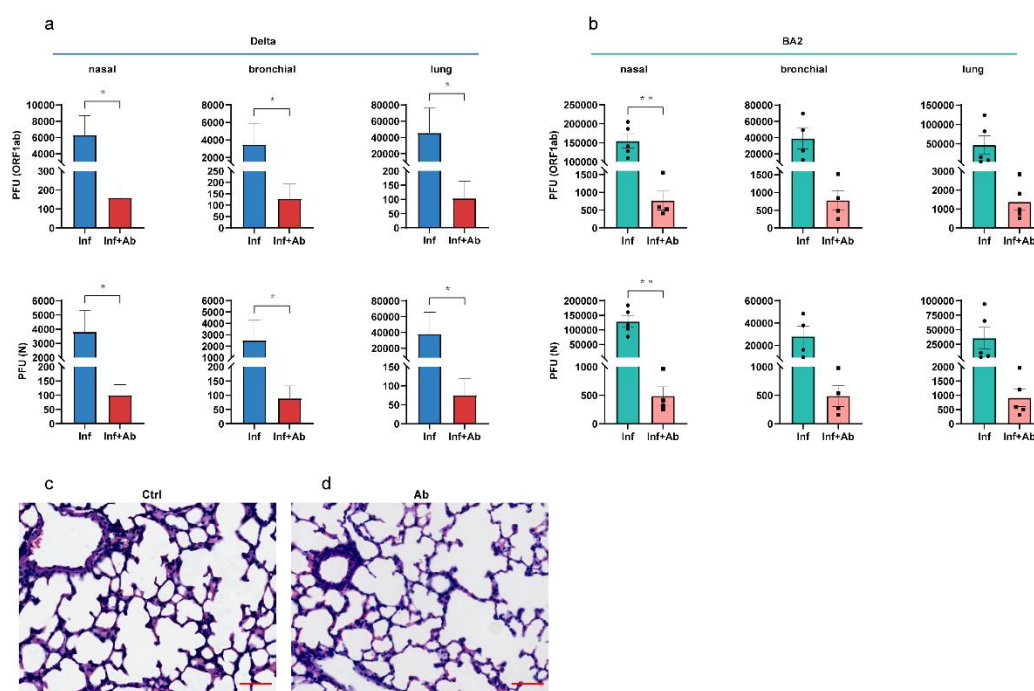
544 **Figure 3:**



545

546 **Figure 3.** 2-D airway organoid and infection model construction from differentiated nasal
547 epitheliums. (a) Representative images of immunofluorescence staining of nasal organoids
548 with ciliated columnar cells stained with AC- α -tubulin (pink), goblet cells stained with
549 Muc5AC (green) and basal cells stained with P63 (yellow). Nucleus were stained by the 4',6-
550 diamidino-2-phenylidole (DAPI). Scale bar = 20 μ m. (b) Representative images of
551 hematoxylin-eosin (H&E) staining of nasal organoids. Scale bar = 50 μ m. (c, d) Representative
552 immunofluorescence staining of nasal organoids infected with mock control or BA.2. Ciliated
553 columnar cells, virus and nucleus were stained for β -Tubulin (pink), SARS-CoV-2 Spike
554 protein (green) and DAPI (blue) respectively. Scale bar = 20 μ m.

555 **Figure 4:**



556

557 **Figure 4.** Anti-RBD-pAb efficiency and safety tests. qPCR quantification of ORF1ab and N
558 domains of SARS-CoV-2 Delta (a) and BA.2 (b) strains in topical secretions of the infected
559 organoids as indicated. H&E-stained lung sections from mice with inhalation of saline control
560 (c) or anti-RBD pAbs (d) showed no significant difference. Scale bar = 50µm.

561